Near-wall investigation of a streamwise vortex pair

by

D.D. Kuhl[1] and R.L. Simpson[2]

Department of Aerospace and Ocean Engineering
Virginia Polytechnic Institute and State University
Blacksburg, Virginia 24061; USA

ABSTRACT

Simultaneous three-orthogonal component LDV measurements with a measurement volume on the order of 50 μm in size were made in a turbulent boundary layer downstream of a pair of half delta-wing vortex generators. Coincident instantaneous U, V, W components of the velocity were used to determine the mean flow, Reynolds stresses, and triple products. Measurements below $y^+ = 5$ were made and used to deduce the wall skin friction. Careful considerations were given to the evaluation of bias and broadening effects on the data. Data for a 2-D turbulent boundary layer closely agree with direct numerical simulation (DNS) results. All turbulence data satisfy the realizability conditions. This is the first time that detailed near-wall measurements have been made in this type of flow. While large streamwise vorticity is generated away from the wall, significant opposite sign vorticity is generated by the viscous interaction of the vortex and the wall. Further analysis of this data set is found in Kuhl (2000).

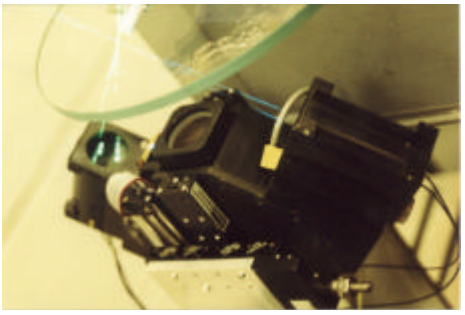

Figure 1: 3-orthogonal-velocity-component fiber-optic LDV head

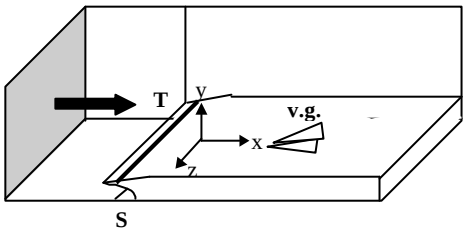

Figure 2: Experimental test set-up showing suction slot S; boundary layer trip T and vortex generator pair v.g.

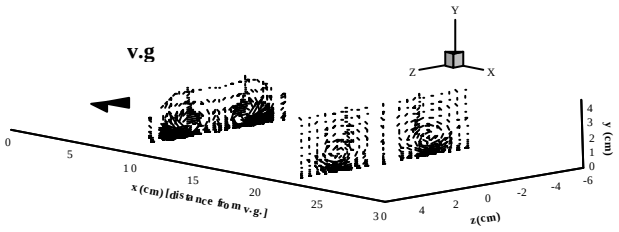

Figure 3: VW mean secondary flow vectors in 2 measurement planes

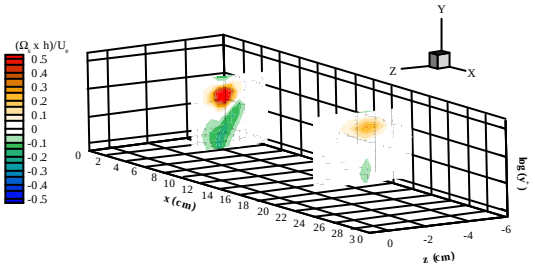

Figure 4: Mean streamwise vorticity for a semi-span in log(y^+) and z planes

[1] Graduate Assistant
[2] Jack E. Cowling Professor

NOMENCLATURE

C	Correlation coefficient
h	Height of Vortex Generator (1 cm).
n	Number of points in ensemble.
r_i	Data rate: $1/(t_i-t_{i-1})$
R	Statistical mean data rate from the selected ensemble: $\sum_{i=1}^{n} \lvert r_i \rvert \Big/ n$
Re_θ	Momentum thickness Reynolds number: $U_\infty \theta / \nu$
Re_x	Reynolds number: $U_\infty x / \nu$
t_i	Absolute time of the ith velocity measured in the selected ensemble
U_e	Freestream Velocity
$\overline{u}, \overline{v}, \overline{w}$	Statistical mean velocity from the selected ensemble in tunnel co-ordinates.
u_i, v_i, w_i	The i^{th} velocity measured in the selected ensemble in tunnel co-ordinates.
$\overline{u^2}, \overline{v^2}, \overline{w^2}$	Statistical mean velocity squared quantities from the selected ensemble in tunnel co-ordinates.
u^+, v^+, w^+	$\overline{u}/U_\tau$, $\overline{v}/U_\tau$, $\overline{w}/U_\tau$
$-\overline{uv}, -\overline{uw}, -\overline{vw}$	Statistical mean shear stress quantities from the selected ensemble in tunnel co-ordinates.
$\overline{u^2 v}, \overline{vw^2}, \overline{v^3}$	Statistical mean triple product quantities from the selected ensemble in tunnel co-ordinates.
U_τ	Skin Friction velocity: $\sqrt{\tau_w / \rho}$
$\lvert \boldsymbol{V} \rvert$	Statistical mean velocity magnitude from the selected ensemble: $\sum_{i=1}^{n} \lvert \boldsymbol{v}_i \rvert \Big/ n$
$\lvert \boldsymbol{v}_i \rvert$	The ith measured velocity magnitude from the selected ensemble: $\left(u_i^2 + v_i^2 + w_i^2\right)^{0.5}$
x, y, z	Tunnel co-ordinate system (see Figure 2).
y^+	yU_τ / ν
Γ_c	Circulation: $\oint \mathbf{V} d\mathbf{s}$ (in the z-y plane)
$\sum_{i=1}^{n}$	Summation from i =1 to n
σ_r	Standard deviation data rate: $\left(\sum_{i=1}^{n} \lvert r_i \rvert^2 \Big/ (n-1) \right)^{1/2}$
σ_v	Standard deviation of velocity magnitude: $\left(\sum_{i=1}^{n} \lvert v_i \rvert^2 \Big/ (n-1) \right)^{1/2}$
ρ	Mass density of flow
ν	Kinematic viscosity
τ_w	Wall shear stress
Ω_x	Vorticity, curl **V:** $\left(\frac{\partial v}{\partial z} - \frac{\partial w}{\partial y} \right)$
ω_x	$(\Omega_x * h)/U_e$

1. INTRODUCTION

The present work is a study of large-scale streamwise vortices in a turbulent boundary layer, being specifically detailed measurements of the structure of the flow downstream of a half-delta wing vortex generator pair. Such previous experimental studies (Pauley and Eaton, 1989) have used hot-wire anemometry to measure the flow velocities. Hot-wire anemometry is of limited use in detecting all three velocity components within the boundary layer near-wall region. The primary focus of the paper is to report fine resolution measurements of stresses and turbulent triple products throughout the boundary layer and especially near the wall.

Figure 2 shows the approximate shape of the test section along with the location of the vortex generators. The vortex generators that have a chord length of 2.5 cm and are 1 cm in height were attached 9 cm downstream of suction slot and designed to produce the common flow directed down towards the wall, otherwise known as "common flow down" shown in Figure 3. The reason for this particular geometry is that it is part of a moving-wall axial pump cascade flow facility.

The present study uses a miniature fiber-optic 3-orthogonal-velocity-component LDV probe described by Chesnakas and Simpson (1994) and shown in Figure 1. Experimental data were taken at three streamwise positions in the tunnel, 7 cm downstream of the suction slot and 10.5 cm and 44.4 cm downstream of the vortex generator pair. The first test position, 7 cm downstream, was simply used as a point to measure the quality of the flow and provide flow information upstream of the vortex generators. The 10.5 and 44.4 cm cross-sections were the two main experimental cross-sections where the vortex turbulence structure was examined.

2. APPARATUS AND TEST FLOW

The measurements were made in the Virginia Polytechnic Institute and State University Small Boundary Layer Tunnel (Smith et. al 1990). This tunnel was recently modified into a continuous closed return tunnel to accommodate the use of particle seeding in the flow.

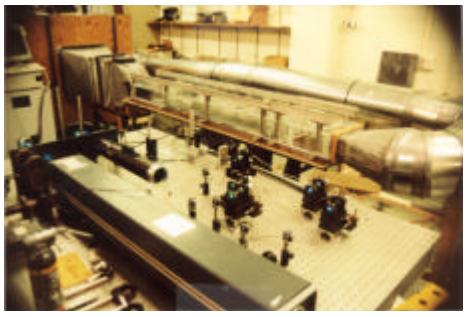

Figure 5: Wind tunnel and test section

The test section is approximately 1.25 m (50 inches) long, 24 cm (9.5 inches) in width and 10 cm (4 inches) in height. A picture of the wind tunnel and test section along with the laser table is shown in Figure 5. The nominal free-stream velocity of the tunnel was 13 m/s for all the runs taken in the tunnel. The stream-wise velocity profile along the length of the test section is shown in Figure 6. A suction slot (Figure 2) is located 9 cm upstream of the vortex generators and is used to remove the upstream boundary layer from the flow. The leading edge has a slight incline before it reaches the tunnel test section floor height (see Figure 2).

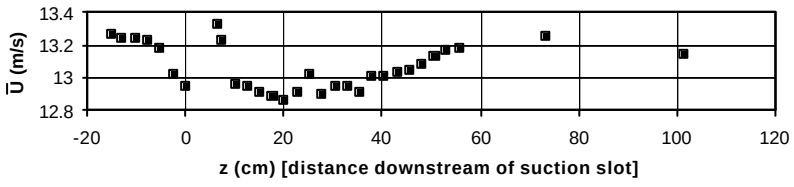

Figure 6: Stream-wise free-stream velocity profile approx. 3 cm above floor of tunnel

A single square bar, 2.4 mm in height, is attached 0.6 cm (0.25 inches) downstream of the suction slot and is used to trip to flow. Several different types of trips were studied before a final trip design was chosen. The range of trips varied from several lines of staggered vertical posts of diameters of the order of 1.5 mm and 0.75 mm, to wires of that same diameter glued to the floor span-wise, to the eventually selected bar that is glued to the floor. The posts were not used

because the flow that was created was highly 3-dimensional in the boundary layer near the vortex generators. The final bar was chosen because of the nicely 2-dimensional boundary layer (Figure 7) it created as well as the desired boundary layer momentum thickness. After the trip was installed Re_θ was determined from measured velocity profiles to be an average of around 700 at a location 7 cm downstream of the suction slot.

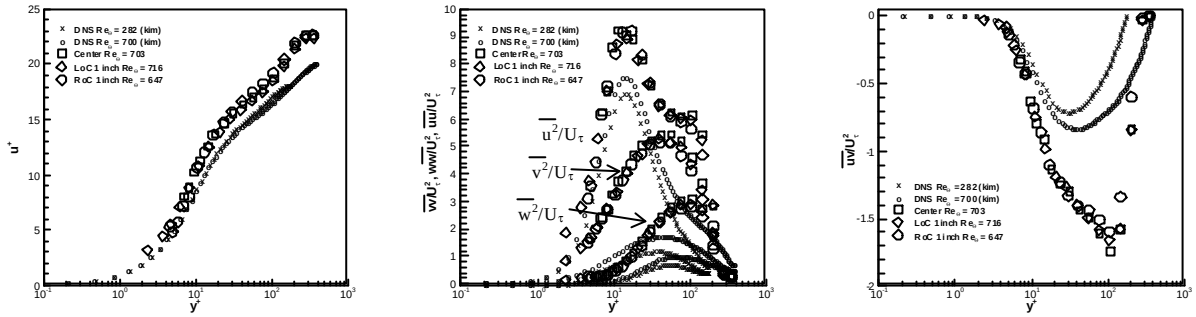

(a) (b) (c)

Figure 7: 7 cm downstream of suction slot, no vortex generators.

Three profiles were taken at 7 cm downstream of the suction slot, one at the center of the tunnel and one 2.54 cm on either side. Figure 7 shows the close two-dimensionality of this flow. In these figures the data are compared with 2-D channel flow DNS results of Kim (1987). Plotted are u^+, $\overline{u^2}/(U_\tau)^2$, $\overline{v^2}/(U_\tau)^2$, $\overline{w^2}/(U_\tau)^2$ and $\overline{uv}/(U_\tau)^2$. Evidently with such a low Reynolds number flow the structure has not completely relaxed at this location. This explains the disagreement with Kim's DNS results shown in Figure 7c and to a lesser extent Figure 7b. This trip however showed the least distortion of the boundary layer of any trips tested which produced the needed Re_θ values. Without vortex generators the profiles match-up almost perfectly with Kim's DNS results 21.8 cm downstream of the suction slot, where Re_θ = 1100. The only reason that the test section 2-dimensional data do not match the DNS results better is due to the difference in Reynolds numbers.

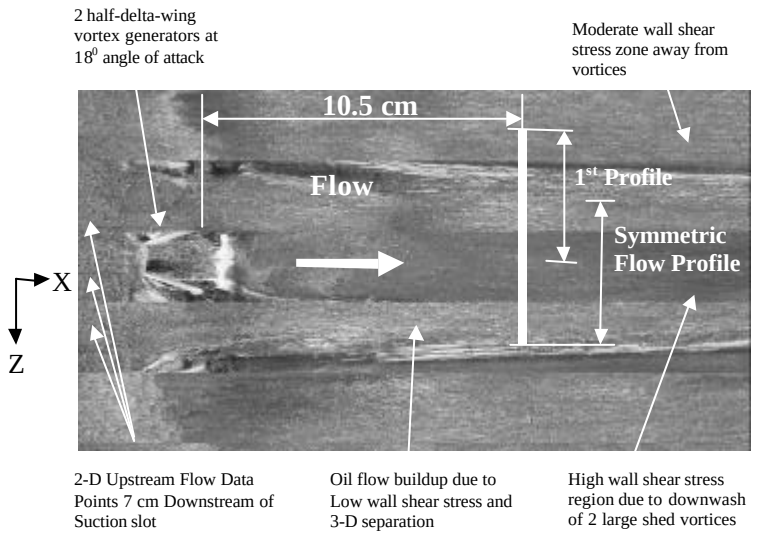

Figure 8: Oil flow visualization

The vortex generators have a chord length of 2.5 cm and are 1 cm in height, which is the same aspect ratio as studied by Pauley and Eaton (1989). The spacing of the generators measured between the midway point of the delta wing chord was 0.8 times the chord, and the angle of attack, as measured between each vortex generators and the tunnel centerline, was 18 degrees, also as studied by Pauley and Eaton. The trailing edge of the vortex generators is 11.3 cm downstream of the suction slot.

Figure 8 shows a surface oil flow on the tunnel floor. From the oil flow you can see that the streaklines in the dark higher shear stress region downstream and between the vortex generators run parallel to the white low wall shear

stress streaklines. This line separates a region of high wall shear stress and that of lower wall shear stress. At the first test profile section (10.5 cm downstream of the vortex generators) the line is at 1.82 cm from the centerline of the tunnel. At the second profile section (44.4 cm downstream of the vortex generators) the line is at 2.81 cm from the centerline of the tunnel.

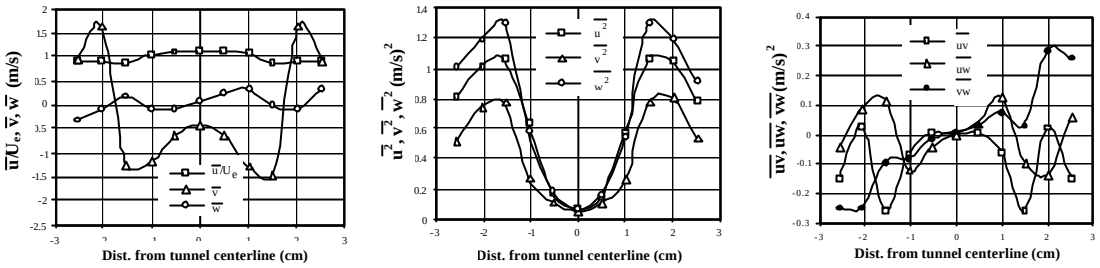

(a) (b) (c)

Figure 9: Tunnel symmetry 10.5 cm downstream of v.g., 0.75 cm off of wall

For the data in Figure 9 the measurement volume was positioned 10.5 cm downstream of the vortex generators and raised to a height of 0.75 cm above the wall. It was then traversed from –2.54 cm to +2.54 cm across the centerline of the tunnel. Plotted are $\overline{u}/U_e$, $\overline{v}$, $\overline{w}$, $\overline{u^2}$, $\overline{v^2}$, $\overline{w^2}$, $\overline{uv}$, $\overline{uw}$ and $\overline{vw}$. As can be seen from these plots the vortices are nearly perfectly symmetrical; therefore, all of the later data were taken only on one half of the tunnel, left of the centerline looking downstream.

Chesnakas and Simpson (1994) describe the laser head, which is a two-color, three-orthogonal-velocity-component, fiber-optic design, shown in Figure 1. The fiber-optics transmit 3 green (514.5 nm) and 2 blue (488 nm) argon-ion laser beams and receive the off-axis backscatter signal through a 6 mm thick optical glass window as the test surface. In this way the flow is undisturbed by the presence of the probe under the tunnel. The probe was mounted to a system of two traverses for the y and z directions, both of which had a travel of +/- 2.54 cm.

The fringe spacing for each pair of laser beams was calculated to be around 5 μm using equations found in Durst et. al. (1981). The crossing of these beams created a nearly spherical control volume of around 50 μm diameter, which was calculated using formula from Durst et. al. (1995). Since the measurements were taken in the same manner as Ölçmen and Simpson (1995), the uncertainties of all of the calculations are assumed to be similar, and are shown in Table 1.

The Doppler frequency of the LDV signals were analyzed using three Macrodyne model FDP3100 frequency domain signal processors operating in coincidence mode. An IBM PC along with a Dostek (1400A Laser Velocimeter Interface with TCEM daughterboard option) was used to collect and store the data from the Macrodynes.

U/U_τ	±0.075	$\overline{u^2v}/U_\tau^3$	±0.039
V/U_τ	±0.026	$\overline{u^2w}/U_\tau^3$	±0.066
W/U_τ	±0.05	$\overline{v^2w}/U_\tau^3$	±0.015
$\overline{u^2}/U_\tau^2$	±0.08	$\overline{uv^2}/U_\tau^3$	±0.016
$\overline{v^2}/U_\tau^2$	±0.029	$\overline{uw^2}/U_\tau^3$	±0.059
$\overline{w^2}/U_\tau^2$	±0.037	$\overline{vw^2}/U_\tau^3$	±0.012
$-\overline{uv}/U_\tau^2$	±0.043	$\overline{uvw}/U_\tau^3$	±0.019
$-\overline{uw}/U_\tau^2$	±0.023	$\overline{u^3}/U_\tau^3$	±0.189
$-\overline{vw}/U_\tau^2$	±0.012	$\overline{v^3}/U_\tau^3$	±0.018
		$\overline{w^3}/U_\tau^3$	±0.051

Table 1: Uncertainties in measured quantities

To seed the flow an aerosol generator designed by Echols and Young (1963) was used. The fluid used in the generator was dioctal phthalate with a mean particle size of about 2 μm. The smoke was injected into the plenum chamber of the wind tunnel.

3. POST-PROCESSING

There are two major steps for the post-processing of the data, the first being preparation of the acquired data and the second being calculation of the desired quantities. The preparation of the data was conducted by addressing the three problem areas in LDV data: noise, signal biasing and broadening effects, and co-ordinate and wall location adjustments. The desired quantities calculated were the mean velocities, turbulent stresses, triple products, vorticity (Ω_x) and circulation (Γ_c).

With any LDV system, like any electronic measurement system, there is always a certain amount of extraneous noise while taking data. The method used to remove noise from the data was the same as used by Ölçmen and Simpson (1995). A parabola was fit to each side of the logarithm of the velocity component histogram ordinate in the range between 1% to 80% of the peak histogram value. The data lying outside of the intersection of the parabolas with the ordinate value = 1 line were discarded; if only one velocity component was deemed bad, all three velocity components for that data point were discarded. The clean velocity information for all three velocity components was transformed into tunnel co-ordinates and saved. Once more a parabola was fit to each side of the logarithm of the histogram, this time to the transformed data, and the noise was removed. The number of samples taken at each point ranged from 15,000 to 30,000.

First the velocity bias was investigated. To assess whether or not there were velocity bias effects in our data a method similar to that of Meyers et. al. (1992) was used. Basically a standard correlation coefficient (C) was calculated for each location in our two test cases (3-D and 2-D). The correlation coefficient was calculated as follows.

$$C = \frac{\sum_{i=1}^{n} \left(|V| - |v_i|\right)\left(R - r_i\right) \Big/ n}{\sigma_v \sigma_r}$$

The measured correlation coefficient for both of our flows are shown in Figure 10 for the two-dimensional case and a three-dimensional case through the vortex center. With all of the correlation coefficients of the order of 10^{-2}, there is no correlation between velocity magnitude fluctuation and data rate fluctuation for either case, and thus no velocity bias.

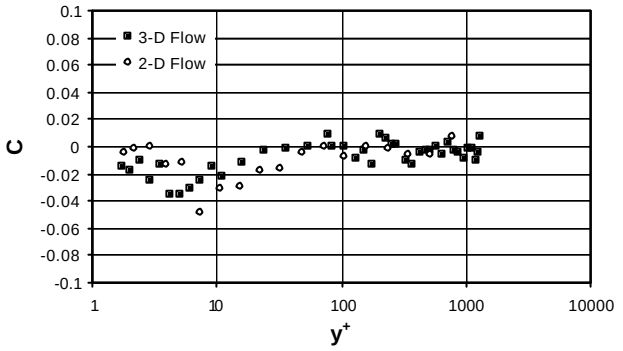

Figure 10: Correlation coefficient

Figure 11 is a plot of the same set of data processed with and without the velocity bias correction of Fuchs

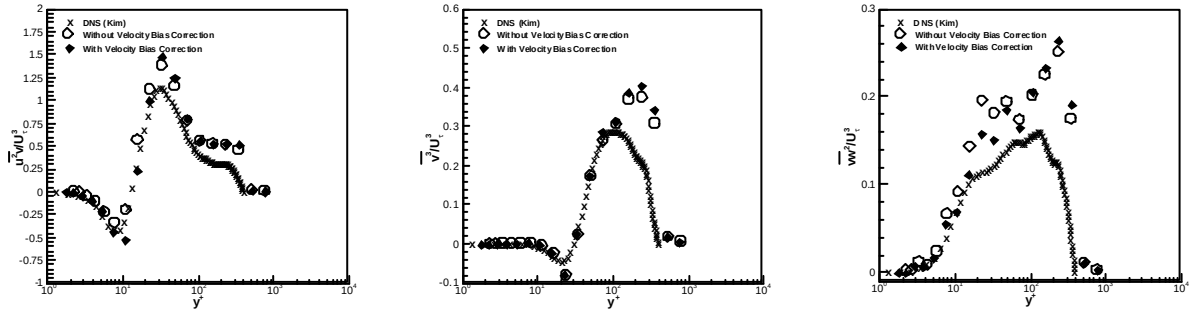

(a) (b) (c)

Figure 11: Velocity bias correction comparison for 2-D flow data, Re_q=1100.

et. al. (1992). The data set chosen was taken at the first experimental test section (10.5 cm downstream of the vortex generators) and in the center of the tunnel. There were no vortex generators in the tunnel so the mean flow was 2-dimensional. Looking at Figure 11 it is clear to see that the velocity bias correction factor had very little effect on the data. It is also clear to point out that these data compare very favorably with Kim's (1987) DNS channel results. Any deviations between the DNS results and the experimental data are explained by the difference in Reynolds numbers. The Reynolds number for the DNS results was Re_θ=700. The Reynolds number for the experimental data was Re_θ=1100. This increased the deviation between the DNS and experimental values away from the wall and near the free-stream. It should be noted that all of the 2-D data was also compared with Spalart's (1988) famous DNS results at Re_θ=1410, which reported no triple products.

Chen et. al. (1996) proposed that for 3-component LDV systems the change in projected area of the coincident measurement volume for different flow directions will introduce an 'angular' bias in naturally sampled data. For the LDV optics used here, there is only a small variation in the measurement volume projected cross-sectional area for the various flow directions. Thus, negligible angular bias is present in the current correlation measurements. The fringe bias effects described by Whiffen et. al (1979) is not present since only particles passing through the coincident measurement volumes are validated. The geometric bias proposed by Brown (1989) is practically removed since the measurement volume is basically spherical.

There are three types of broadening effects which need to be addressed: velocity gradient broadening, finite transient time broadening, and instrument broadening effects. Velocity gradient broadening occurs because the LDV system receives signals over the measurement volume in a flow with velocity gradients. However, with a small enough measurement volume this effect can be greatly reduced. Using equations suggested by Durst et. al. (1992) the effect of gradient broadening could be calculated. The effect of gradient broadening was found to be orders of magnitude less than the uncertainty in the data.

To measure the effect of transient time broadening, the data were compared with the Ma et. al. (2000) data. Ma measured the same outer region flow at the same cross-sections except using hot-wire anemometry. When the two data sets were compared it was found that there was negligible differences in the measured velocities. Therefore, it was concluded that the effect of transient time broadening on the data was insignificant. Ölçmen studied the instrument broadening effects for this system and found that the bandwidth broadening of the Macrodyne signal processors contribute a negligible amount of broadening to the signal (Ölçmen et. al. 1998).

When the measurement volume is focused just onto the surface, a strong signal results that determines an approximate reference location for the LDV head traversing system. A more refined determination of the measurement volume location relative to the wall can be determined by a least squares curve fit of the sublayer mean velocity profile:

$$Q = C_1 * y + C_2 * y^4$$

with $Q = \left(\overline{u}^2 + \overline{w}^2\right)^{1/2}$, and C_1 and C_2 as coefficients. The curve is fit through Q=0 at y=0. Using only the data for y^+<10, an iterative process was set-up to maximize the curve fit correlation coefficient by adjusting the y values. This was performed at each of the profiles using at least 5 points. Most of the y shifts were of the order of 50 μm, the size of the measurement volume.

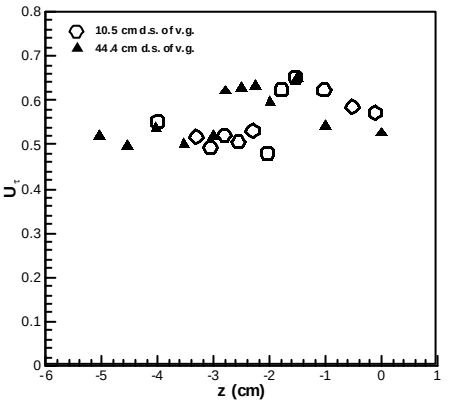

Figure 12: Wall shear stress across tunnel

Using the curve fit above $\tau_? = \mu \left.\frac{\partial \overline{u}}{\partial y}\right|_{wall}$ can be determined using a similar method to that of Durst et. al. (1996). The first coefficient in the above equation relates to U_τ by: $C_1 = U_\tau^2/\nu$. See Kuhl (2000) for more details. Looking at Figure 12 there is a sharp change

in U_τ at z = -1.8 cm for the first cross section at 10.6 cm downstream of the vortex generator. Then for the 44.4 cm cross section the sharp change in U_τ comes at z = -2.8 cm. Both of these values correspond to the sharp contrast of light and dark found on the oil flow in Figure 8 above.

When setting up the LDV head there is no way to avoid slight misalignment of the co-ordinate system for the LDV head relative to the tunnel co-ordinate system. A procedure was set-up to determine the transformation. Each time the probe head was moved a two-dimensional flow case was measured, i.e. the vortex generators were removed and a velocity profile was taken. An iterative process was set-up to rotate the co-ordinate system pitch angle for these data until the $\overline{v}$ values reached a minimum value, within a tolerance. Next the co-ordinate system yaw angle was adjusted until the combination of $\overline{w}$ and $\overline{uw}$ had reached a minimum value within a tolerance. Finally the co-ordinate system roll angle was adjusted until $\overline{vw}$ had reached a minimum value within a given tolerance. Once the LDV head to tunnel co-ordinate system transformation was determined it was applied to all of the three-dimensional data sets until the head was moved to another x location, at which time a new co-ordinate transformation was determined. The angle adjustments were usually on the order of around 1 degree.

Confidence in the post processing schemes can be found in the plots in Figure 11 as well as in Figure 14. There is close agreement between the experimental and DNS results near the wall. These plots confirm the low uncertainties in all of the calculated quantities as given by Ölçmen and Simpson (1995) and shown in Table 1 above.

4. EXPERIMENTAL DATA

All turbulence results satisfy the realizability conditions of Schumann (1977). Figures 13 and 14 show the results from some comparisons between a two-dimensional case and a purely 3-dimensional case. The two-dimensional case data were taken without vortex generators at 10.5 cm downstream of the vortex generator location in the center of the tunnel. The 3-dimensional case was taken as well at 10.5 cm downstream of the vortex generators but it was taken at 1.8 cm left of center (or –1.8 cm in the z tunnel co-ordinates). The 3-dimensional profile position was located almost exactly in the center of the vortex, 1.77 cm from the centerline.

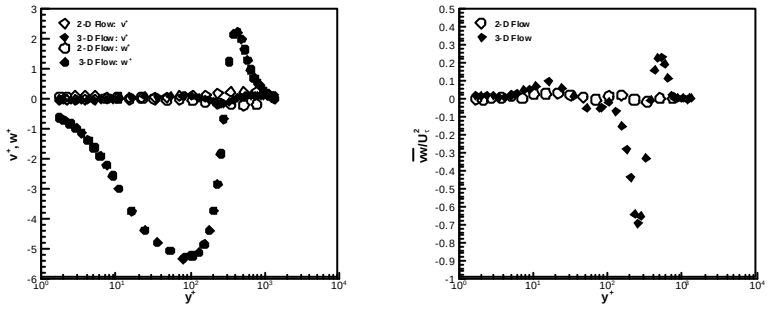

(a) (b)

Figure 13: Secondary flow plots

Figure 13a shows the secondary flow components. The first plot shows how well the 2-D data remains at zero and how the 3-D v^+ component is really quite negligible compared to w^+, as would be expected in the plane cutting the center of the vortex. From figure 13a we can determine the center of the vortex. The profile is for the z position that passes directly through the center of the vortex, so the w=0 location is at the center of the vortex. As was stated above it was interpolated that the center of the vortex is at y^+= 295.4.

Figure 13b shows some interesting behavior near the wall for the spanwise shearing stress $-\overline{vw}$, where major terms of the $-\overline{vw}$ transport equation are production and diffusion: $\overline{v^2}\frac{\partial W}{\partial y} = \frac{\partial}{\partial y}\left(-\overline{v^2 w}\right)$.

Therefore we see the slight rise in $-\overline{vw}$ around $y^+<11$ is due to production of $-\overline{vw}$ and then a reduction at higher y^+ is due to the vortex production and diffusion.

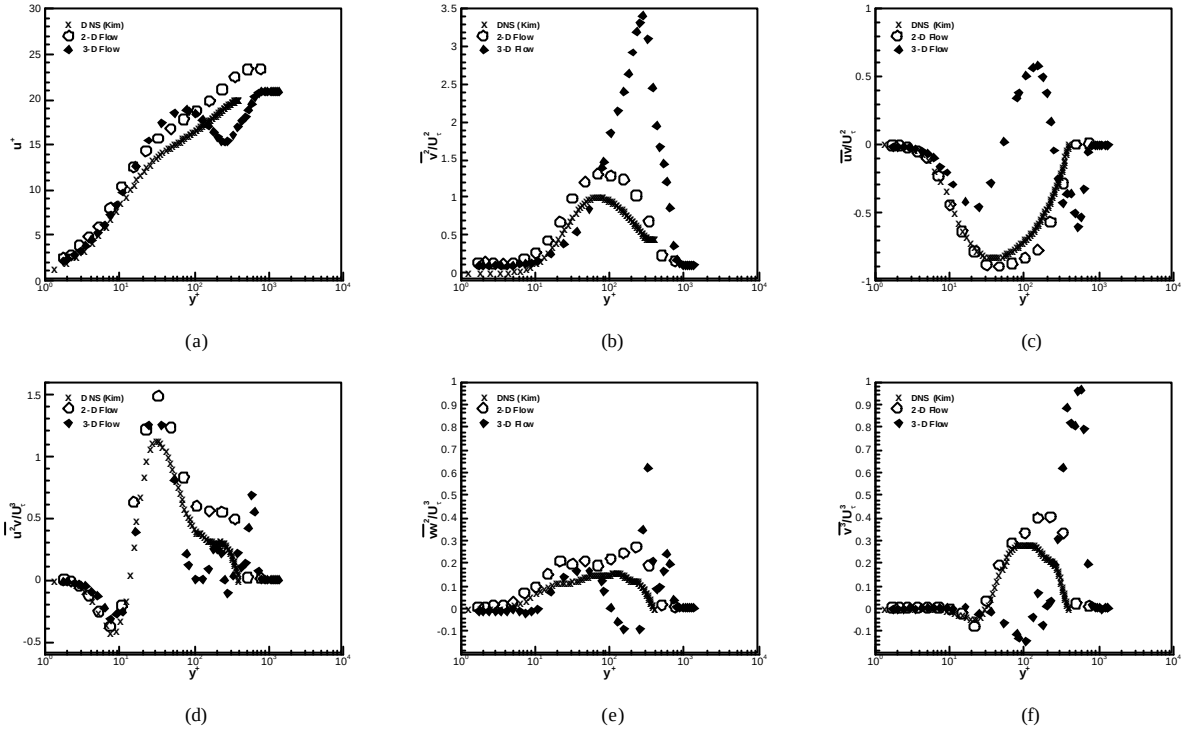

Figure 14: Comparison of 2-D (Re_q=1100), DNS results (Re_q=700) and 3-D results through vortex core

Looking at Figure 14 there is much to be noted in each of the plots. Figure 14a shows the plot of the u^+. As has been noted above the 2-dimensional plot closely follows the DNS results (Kim 1987) near the wall but rises up as it gets to the outer portion of the boundary layer. Again, this is explained as a difference of Reynolds numbers, the DNS's Re_θ=700 verses the experimental Re_θ=1100. The dip in the velocity for the 3-D case in this plot shows the decrease in the streamwise velocity through the core of the vortex. This is nicely contrasted with the log region of the 2-D profile.

Looking at Figure 14b a peak in $\overline{v^2} / U_\tau^2$ is noted around y^+=295, which we determined above from Figure 13a, is the center of the vortex. It should be noted in Figure 14c how well the DNS results follows the experimental 2-D data. The peak for the $-\overline{uv}$ ends up being below the peak $\overline{v^2}$ that is near y^+=80.

Figures 14d-f show close agreement between all profiles near the wall. As the 3-dimensionality of the vortex becomes dominant the plots quickly diverge. Figure 14f shows a large amount of transport of the turbulent kinetic energy out towards the freestream. For all of these plots it should be noted that the small variations for the most part in all of the plots are real phenomena and not random jitter (see Ölçmen and Simpson 1995) A full analysis of the meaning of the triple product results will be done in Kuhl (2000).

Circulation was calculated in both of the planes of data using a numerical integration around the outer edge of the flow field. Since the vortices were roughly perpendicular to the test section the circulation was calculated in the z-y plane. The circulation was normalized on the average freestream velocity over all of the profiles and with the height of the vortex generators (h=1cm). For the first cross-section (10.5 cm downstream of vortex generators) was Γ_c=-0.18. For the second cross-section (44.4 cm downstream of the vortex generators) the circulation decreased to Γ_c=-0.12

The last sets of figures show the results from the data collected at the two streamwise positions, 10.5 cm and 44.4 cm downstream of the vortex generators. Figure 15 a and b show the $\overline{v} - \overline{w}$ mean secondary flow streamlines at the two cross sections. The spanwise or z locations where U_τ in Figure 12 changes abruptly is near where the secondary flow velocities near the wall also change significantly. As can be seen from these plots the center of the vortex moves up and away from the wall as it moves downstream as well as gets larger.

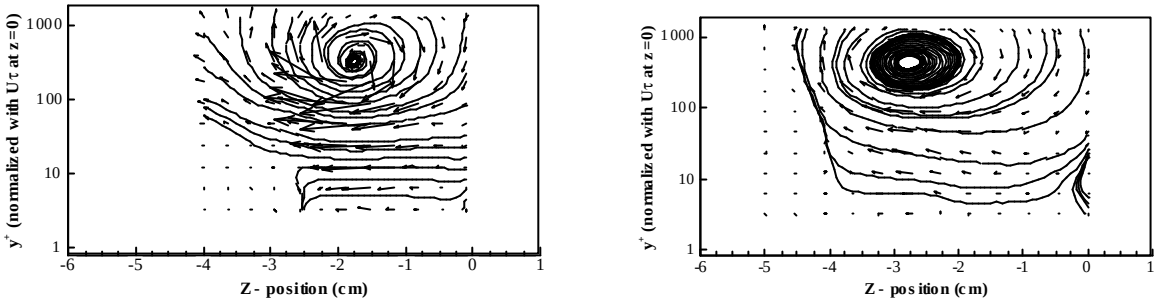

(a) 10.5 cm downstream of v.g. **(b) 44.4 cm downstream of v.g.**

Figure 15: Log y^+ secondary flow (v w) streamlines

Figure 16 a and b show the vorticity contours for the two streamwise positions. The peak vorticity decreased as the flow went downstream. The peak vorticity at the 10.5 cm cross section is estimated to be 0.746. The peak vorticity at the 44.4 cm cross-section is estimated to be 0.284. As reported by Pauley and

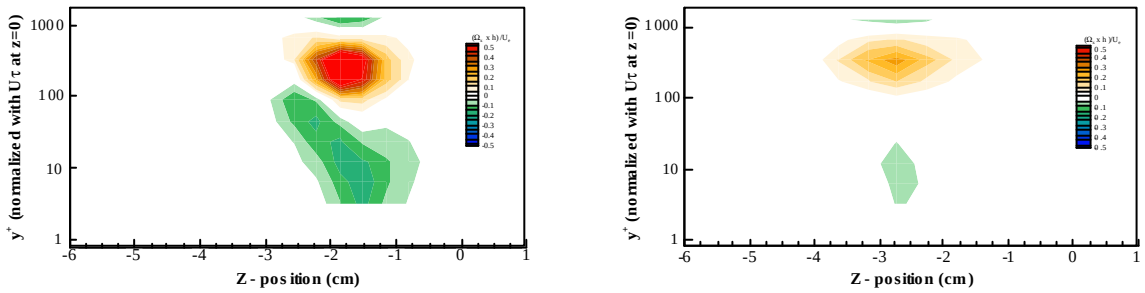

(a) 10.5 cm downstream of v.g. **(b) 44.4 cm downstream of v.g.**

Figure 16: Log y^+ streamwise vorticity w_x

Eaton (1989), there is significant opposite sign or "induced" streamwise vorticity generated by the viscous interaction of the vortex and the wall.

5. CONCLUSIONS

The velocity structure of a boundary layer with a streamwise vortex pair has been measured using a 3-orthogonal-velocity–component fiber-optic LDV system with a 50 μm measurement volume. There is no significant correlation between data rate fluctuations and velocity fluctuations. Results for a 2-D turbulent boundary layer agree closely with those from a DNS, which confirms that velocity bias and signal broadening effects are negligible. While large streamwise vorticity is generated away from the wall,

significant opposite sign vorticity is generated by the viscous interaction of the vortex and the wall. It was found that an abrupt step change in the wall shear stress magnitude occurs just outside of the vortex center. Further analysis of this data set is found in Kuhl (2000).

ACKNOWLEDGEMENTS

The authors appreciate the support of the Office of Naval Research through Dr. Edwin Rood, Program Manager. Dr. Semih Ölçmen resurrected the LDV system for the current work. These data will be available on the webpage: http://www.aoe.vt.edu/aoe/faculty/rogfac.html.

REFERENCES

Brown, J.L., 1989, "Geometric bias and time coincidence in 3-dimensional laser Doppler velocimeter system," *Experimental Fluids* Vol. 7, pp. 25-32.

Chen, C.-Y., Kim, P.J., and Walker, D.T. 1996 "Angular Bias Errors in Three-Component Laser Velocimeter Measurements," *J. Fluids engineering*, Vol. 1188, pp.555-561.

Chesnakas, C.J., and Simpson, R.L., 1994 "Full three-dimensional measurements of the cross-flow separation region of a 6 : 1 prolate spheroid," *Experiments in Fluid* Vol. 17, pp. 68-74.

Durst, F., Jovanovic, J., and Sender, J., 1995 "LDAmeasurements in the near-wall region of a turbulent pipe flow," *Journal of Fluid Mechanics* Vol. 295, pp. 305-335.

Durst, F. Kikura, H., Lekakis, I., Jovanovic, J., and Ye, Q., 1996 "Wall shear stress determination from near-wall mean velocity data in turbulent pipe and channel flows," Experiments in Fluids, 20, pp. 417-428

Durst, F., Martinuzzi, R., Sender, J., and Thevenin, D., 1992 "LDA-Measurements of Mean Velocity, RMS-Values and Higher Order Moments of Turbulence Intensity Fluctuations in Flow Fields with Strong Velocity Gradients," Proceedings of the 6th International Symposium on Applications of Laser Techniques to Fluid Mechanics, Lisbon, Portugal, paper 5.1.1.

Durst, F., Melling, A., and Whitelaw, J.H., 1981 Principles and Practice of Laser-Doppler Anemometry, Second ed., Acad. Press, p. 32.

Echols, W.H., and Young, J.A., 1963 Studies of portable air-operated aerosol generator, *NRL Report,* 5929.

Fuchs, W., Albrecht, H., Nobach, H., Tropea, C. and Graham, L.J.W., 1992 "Simulation and experimental verification of statistical bias in laser Doppler anemometry including non-homogenous particle density," Proceedings of the 6th International Symposium on Applications of Laser Techniques to Fluid Mechanics, Lisbon, Portugal, paper 8.2.1.

Kim, J., Moin, P. and Moser, R.,1987 "Turbulence statistics in fully developed channel flow at low Reynolds number", *Journal of Fluid Mechanics* Vol. 177, p. 133.

Kuhl, D., 2000, M.S. Thesis, Virginia Polytechnic and State University, Aerospace and Ocean Engineering Department.

Ma, R., Saha, N., Devenport, W.J., and Wang, Y., 2000 "Unsteady Behavior of a Tip Leakage Vortex Produced by Simulated Stator/Rotor Interaction," AIAA paper 2000-2217, Fluids 2000, Denver, CO, June 19-22.

Meyers, J.F., Kjelgaard, S.O., and Hepner, T.E. 1992 “Investigation of Particle sampling Bias in the Shear Flow Field Downstream of a Backward Facing Step” Proceedings of the 6th International Symposium on Applications of Laser Techniques to Fluid Mechanics, Lisbon, Portugal, paper 29.1.

Ölçmen, S.M., and Simpson, R.L. 1995 “A five-velocity –component laser-Doppler velocimeter for measurements of a three-dimensional turbulent boundary layer,” *Measurement Science and Technology*, Vol. 6, pp. 702-716.

Ölçmen, S.M., Simpson, R.L., and Goody, M. 1998 “An Experimental Investigation of Two-Point Correlations in Two- and Three Dimensional Turbulent Boundary Layers,” AIAA paper 98-0427, 36th Aerospace Sciences Meeting and Exhibit, Reno, NV, January 12-15.

Pauley, W.R., and Eaton, J.K., 1989 “Boundary Layer Turbulence Structure in the Presence of Embedded Streamwise Vortex Pairs,” Seventh Symposium on Turbulent Shear Flows, Stanford University, August 21-23.

Schumann, U., 1977 “Realizability of Reynolds-stress turbulence models,” The Physics of Fluids, Vol 20, No. 5, May 1977.

Smith, E.J., Rife, M.C., and Devenport, W.J. 1990 Investigation of the Small Boundary Layer Tunnel, Aerospace and Ocean Engineering Department, Virginia Polytechnic Institute and State University Report VPI-AOE-175, July 17.

Spalart, P.R. 1988 “Direct simulation of a turbulent boundary layer up to R=1410.” Journal of Fluid Mechanics, Vol.187, p. 61

Whiffen, M.C., Lau, J.C., and Smith, D.M., 1979 “Design of LV Experiments for Turbulence Measurements,” *Laser Velocimetry and Particle Sizing*, Thompson, H.D. & Stevenson, W.H., eds. Hemiphere, pp. 197-207.